TITLE
ASP Conference Series, Vol. **VOLUME***, **YEAR OF PUBLICATION**
NAMES OF EDITORS

Mechanisms of Chromospheric and Coronal Heating

Peter Ulmschneider

Institut of Theoretical Astrophysics, University of Heidelberg, Tiergartenstr. 15, 69121 Heidelberg, Germany

Zdzislaw Musielak

Department of Physics, University of Texas at Arlington, Arlington, TX 76019, USA

Abstract.

Practically all stars are surrounded by very hot layers where the temperature can reach values almost as high as in the stellar core. These layers are responsible for the observed X-ray, UV and radio emission and are also essential for the mass-loss by stellar winds. It can now be said with some confidence that the chromosphere is heated by waves. Acoustic waves appear to be the basic heating mechanism for nonmagnetic regions while longitudinal tube waves, generated either directly or from transverse and torsional tube waves via nonlinear mode-coupling, are responsible for the heating of magnetic regions. It appears that starting at the highest chromospheric layers and the chromosphere-corona transition region the heating by waves produced in the convection zone becomes insufficient and reconnection (microflares) is likely to be an additional important heating mechanism there. We discuss the tedious quest for the identification and understanding of the basic heating mechanisms that generate these surprisingly hot outer stellar layers.

1. Inventory of mechanical heating mechanisms

Chromospheres and coronae are stellar layers where extensive mechanical heating takes place (e.g., Narain & Ulmschneider 1996). To accomplish this heating various mechanisms have been proposed which all are known to work in a terrestrial laboratory. Table 1 shows a summary of proposed mechanisms which can be classified as hydrodynamic mechanisms and magnetic mechanisms. The magnetic mechanisms can be further subdivided into AC-mechanisms or waves and DC-mechanisms or magnetic field dissipation mechanisms. The left hand column of Tab. 1 lists the carriers of mechanical energy while the right hand column shows the processes by which these carriers heat.

The hydrodynamic mechanisms consist of acoustic waves with periods less than the acoustic cut-off period P_A (see Eq. (3) below) and pulsational waves with periods larger than P_A. While the former are generated by the turbulent motions in the convection zone, the latter, well known for instance from Mira pulsations, are generated by the kappa-mechanism (periodic blocking of the

energy carrier	*dissipation mechanism*
hydrodynamic heating mechanisms	
acoustic waves, $P<P_A$	shock dissipation
pulsational waves, $P>P_A$	shock dissipation
magnetic heating mechanisms	
1. alternating current (AC) or wave mechanisms	
slow mode mhd waves, longitudinal mhd tube waves	shock dissipation
fast mode mhd waves	Landau damping
Alfvén waves (transverse, torsional)	mode-coupling resonance heating compressional viscous heating turbulent heating Landau damping
magnetoacoustic surface waves	mode-coupling phase-mixing resonant absorption
plasma waves	ion-cyclotron resonance heating
2. direct current (DC) mechanisms	
current sheets	reconnection (turbulent heating, wave heating)

Table 1. Proposed chromospheric and coronal heating mechanisms, modified after Ulmschneider (1996).

transfer of the stellar radiation by the temperature and pressure dependence of the opacity). Both wave types produce shocks and dissipate their energy by shock dissipation.

For the AC-mechanisms one has slow, fast and Alfvén mode MHD waves in homogenous magnetic fields and longitudinal, transverse and torsional waves in magnetic flux tubes. Figure 1b shows these different tube wave modes and Fig. 1a explains their generation in the turbulent flow fields of the convection zone. It is well known (e.g., Stein & Nordlund 1990) that the gas brought up by the convective bubbles (granulation) flows back into the Sun not in a laminary fashion but in a very turbulent way preferentially in certain downflow regions. Due to the conservation of angular momentum, these flows converging to a small region from a large area on a rotating star, are helical and represent tornados that entrap the magnetic flux tube in its core. These turbulent helical downflows generate three tube wave modes by squeezing, bending and twisting the magnetic flux tube. Very similar to acoustic waves, longitudinal tube waves dissipate their energy by forming shocks, while the transverse and torsional waves most likely dissipate their energy by nonlinear mode-coupling to longitudinal waves although there are also several other dissipation mechanisms (see Tab. 1). Surface waves are certainly present at the boundary of flux tubes but the question is how important they can be for the heating of the entire tube. At great height in the chromosphere plasma waves become important and they can heat the background medium by ion-cyclotron resonance and Landau damping.

The DC-mechanisms heat by reconnection, that is, direct magnetic field dissipation. This happens when by large scale flows (e.g., during flux emergence)

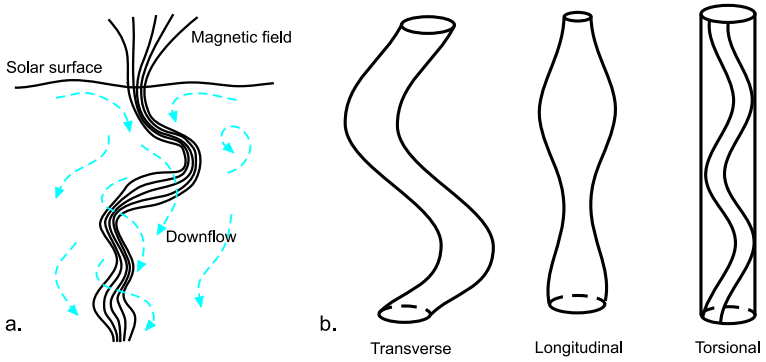

Figure 1. Magnetic tube wave energy generation, after Parker (1981) (left) and tube wave modes (right).

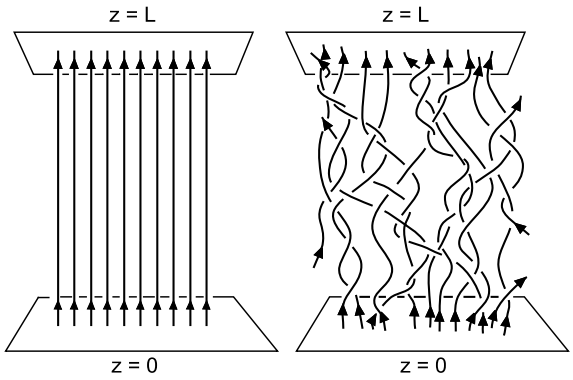

Figure 2. Reconnective heating by foot point motions, after Parker (1991). Minimum energy configuration (left) where excess magnetic energy is stored by braiding and entwining (right).

oppositely directed fields come in close contact like when sunspots, poores or flux tubes get pushed together or when small scale flows like in foot point motions entwines closed loops. Figure 2 shows the situation for a forest of closed magnetic loops which have both foot points ankered in photospheric regions. The foot point motion working on both legs of the loops increases the energy stored in the entwined field. This buildup can only be halted and the field can only return to a minimum energy configuration if reconnections happen. It is thought that these small and frequent reconnection events give rise to microflare heating (e.g., Narain & Ulmschneider 1996).

For understanding chromospheres and coronae it is very important to identify which of these proposed energy carriers is dominant in a given layer, that is, how much energy is produced by each carrier, how it is transported and finally dissipated. This identification process is difficult because the dissipation mechanisms often occur at very small spatial scales that cannot be observationally resolved even for our Sun (Narain & Ulmschneider 1996). Therefore, it is not surprising that the main heating mechanisms operating in the solar and stellar chromospheres and coronae still remain elusive.

How much mechanical energy do we need?		
	$erg\ cm^{-2}s^{-1}$	
VAL-C	$1.4 \cdot 10^7$	Anderson, Athay (1989)
interconnecting loops	$5 \cdot 10^5$	Priest (1982)
quiet region loops	$1 \cdot 10^6$	
active region loops	$1 \cdot 10^7$	
quiet regions	$4 \cdot 10^6$	Withbroe, Noyes (1977)
active regions	$3 \cdot 10^7$	
How much mechanical energy do we have?		
1. magnetic field dissipation		
flux emergence	$4 \cdot 10^6 - 4 \cdot 10^7$	Rempel (2002)
foot point motion	$10^6 - 10^7$?	
2. acoustic waves		
acoustic waves	$1.7 \cdot 10^8$	Ulmschneider, Theurer, Musielak (1996)
3. magnetic waves		
longitudinal tube waves	$1 \cdot 10^7 = 5 \cdot 10^8\ f$	Ulmschneider, Musielak, Fawzy (2001), f=0.02
transverse tube waves	$3 \cdot 10^8 = 1.5 \cdot 10^{10}\ f$	Ulmschneider, Musielak (1998), f=0.02
torsional tube waves	$1 \cdot 10^8$?	

Table 2. Inventory of empirical and theoretical mechanical energy fluxes for the Sun

2. Mechanical energy requirements

Table 2 provides an inventory of the semiempirically determined mechanical energy requirements of solar chromospheric and coronal features. It also shows theoretically determined mechanical energy fluxes of various carriers in the Sun. It is surprising that the amount of energy emitted by regions of the solar atmosphere (several times $10^7\ erg\ cm^{-2}s^{-1}$) is roughly a factor of ten lower than the amount of energy supplied by different carries. The difference could be due to the low accuracy of both the empirical and theoretical estimates, but one also has to take into account the fact that a lot of produced energy will probably not be directly dissipated and but instead it will return to the solar interior, for example, at the other foot point of a closed coronal loop.

The VAL-C energy fluxes of Tab. 2 are based on a semi-empirical solar model and are corrected for the missing Fe line emission. However, one presently does not know how accurate these values are because of the extensive time-dependence of the chromosphere (Carlsson & Stein 1995). The typical radiative energy losses from magnetic features amounts to a few times $10^7\ erg\ cm^{-2}s^{-1}$.

3. Generation of mechanical energy

Starting with the DC-mechanisms one has energy generation due to flux emergence and due to foot point motions. For the former, Rempel (2002) has provided the following estimate. Assume that the total magnetic flux which has emerged over the 11 year sunspot cycle originates from a spherical shell of thickness d in the overshoot layer, where the magnetic field is wound toroidally around the

Sun, and where one has a field strength B. Then the total amount of mechanical energy E available from this flux emergence is

$$E = 4\pi R^2 d\ f\frac{B^2}{8\pi} = \frac{1}{2\pi}RB\ (\pi dRfB) = \frac{1}{2\pi}\ RB\Phi \tag{1}$$

where f is the fraction of the field which emerges, R is the radius of the overshoot layer and $\Phi = \pi dRfB = 10^{24}\ Mx$ is the observed emergent flux over a sunspot cycle. Note that the half cross-section of the shell is $(\pi R^2 - \pi(R-d)^2)/2 \approx \pi dR$). The mechanical energy flux from this flux emergence is then $F_{Em} = E/(4\pi R_\odot^2 t_{11}) = 4\cdot 10^6$ to $4\cdot 10^7\ erg\ cm^{-2}s^{-1}$, where $R_\odot$ is the radius of the Sun and $t_{11} = 3\cdot 10^8\ s$ is the duration of the sunspot cycle. For the mechanical energy flux generated by foot point motions no reliable estimate is available and one probably can use values of the order 10^6 to $10^7\ erg\ cm^{-2}s^{-1}$ (Narain & Ulmschneider 1990, 1996).

Acoustic and magnetic waves are efficiently generated by turbulent flows in the convection zone. Two methods are employed to calculate the resulting wave energy fluxes. With an *analytic approach*, one solves wave equations with suitable source terms. This approach is valid for small amplitude fluctuations. Another method is to use a magnetic flux tube model and apply time-dependent perturbations that represent the external flow fields. This is called the *numerical approach*.

In a convection zone let ρ_0 be the mean density, p_0 the gas pressure, H the scale height, c_S the sound speed, γ the ratio of specific heats and u the flow velocity of the convective motions computed using a convection zone model that is calculated by specifying the star's gravity g, effective temperature T_{eff} and metallicity Z_M. To compute a model of vertically oriented and thin magnetic flux tube, one needs to also specify the field strength B_0 and the tube diameter that is usually taken to be equal to the scale height H at the stellar surface. The physical parameters inside the tube at other heights are then computed assuming the horizontal pressure balance and magnetic flux conservation. Considering a wave with the gas velocity v and pressure perturbation p, the analytical approach gives the following inhomogeneous wave equations for different wave modes.
a. *Acoustic wave generation:*

$$\left[\frac{\partial^2}{\partial t^2} - c_S^2\nabla^2 + \omega_S^2 - c_S^2\omega_{BV}^2\left(\frac{\partial}{\partial t}\right)^{-2}\left(\frac{\partial^2}{\partial x^2}+\frac{\partial^2}{\partial y^2}\right)\right] p_1(\vec{x},t)$$

$$= \frac{1}{c_S\sqrt{\gamma p_0}}\left[c_S^2\left(1+\left(\frac{\partial}{\partial t}\right)^{-2}\omega_{BV}^2\right)\nabla\cdot\nabla\cdot(\rho_0\vec{u}\vec{u}) + \right.$$

$$\left.(\gamma-1)g\left(1+\left(\frac{\partial}{\partial t}\right)^{-2}\vec{g}\cdot\nabla\right)\nabla\cdot(\rho_0 u_z\vec{u})\right] \tag{2}$$

where $p_1 = p/\sqrt{p_0}$ is the normalized pressure perturbation and

$$\omega_S \equiv \frac{c_S}{2H} = \frac{2\pi}{P_S}, \qquad \omega_{BV} \equiv \frac{c_S\sqrt{\gamma-1}}{\gamma H} \tag{3}$$

are the acoustic cut-off frequency and the Brunt-Väisälä frequency, respectively (Musielak et al. 1994).

b. *Longitudinal tube wave generation:*

$$\left[\frac{\partial^2}{\partial t^2} - c_T^2\frac{\partial^2}{\partial z^2} + \omega_D^2\right] p_2(z,t) = \frac{\rho_e}{2\sqrt{\rho_0 B_0}}\frac{c_T^2}{c_A^2}\left(\frac{\partial^2}{\partial t^2} + \omega_{BV}^2\right) u^2(z,t) \qquad (4)$$

where $p_2 = p/\sqrt{\rho_0 B_0}$ and

$$c_T = \frac{c_S c_A}{\sqrt{c_S^2 + c_A^2}}\ , \qquad c_A = \frac{B_0}{\sqrt{4\pi\rho_0}}, \qquad \omega_D = \frac{c_T}{H}\left[\frac{9}{16} - \frac{1}{2\gamma} + \frac{c_S^2}{c_A^2}\frac{\gamma-1}{\gamma^2}\right]^{1/2} \qquad (5)$$

are the tube speed, the Alfvén speed and the Defouw frequency (Defouw 1976), respectively (Musielak et al. 1995). Here subscript 0 stands for the inside, and e for the outside of the magnetic tube.

c. *Transverse wave generation:*

$$\left[\frac{\partial^2}{\partial t^2} - c_K^2\frac{\partial^2}{\partial z^2} + \omega_K^2\right] v_1(z,t) = \frac{\rho_0^{1/4}\rho_e}{\rho_0+\rho_e}\left(\frac{u_z}{H} - \frac{\partial u_z}{\partial z}\right)\left(\frac{\partial}{\partial t}\right)^{-1}\left(\frac{\partial^2 u_x}{\partial t^2} + g\frac{\partial u_x}{\partial z}\right) \qquad (6)$$

where $v_1 = \rho_0^{1/4} v_x$ and

$$c_K = \frac{B_0}{\sqrt{4\pi(\rho_e+\rho_0)}}\ , \qquad \omega_K = \frac{c_K}{4H} \qquad (7)$$

are the kink speed, and the kink frequency, respectively (Musielak & Ulmschneider 2001). Note that different pressure and velocity normalizations were required to cast the wave equations in the Klein-Gordon form.

The acoustic, F_S, longitudinal, F_T, and transverse, F_K, wave energy flux can then be written as

$$F_S = < p\ v >= \sqrt{p_0} < p_1\ v > \qquad (8)$$

with the velocity perturbation, v, given by

$$v = -\frac{\sqrt{p_0}}{\rho_0}\left(\frac{\partial}{\partial t}\right)^{-1}\left[\frac{\partial}{\partial x} + \frac{\partial}{\partial y} + \left(1 + \omega_{BV}^2\left(\frac{\partial}{\partial t}\right)^{-2}\right)^{-1}\left(\frac{\partial}{\partial z} - \frac{2-\gamma}{2\gamma H}\right)\right] p_1\ , \qquad (9)$$

$$F_T =< p\ v_z >= \sqrt{\rho_0 B_0} < p_2\ v_z > \qquad (10)$$

with the longitudinal (vertical) velocity perturbation, v_z, given by

$$v_z = -\sqrt{\frac{B_0}{\rho_0}}\left(\frac{\partial}{\partial t}\right)^{-1}\left[1 + \omega_{BV}^2\left(\frac{\partial}{\partial t}\right)^{-2}\right]^{-1}\left(\frac{\partial}{\partial z} + \frac{4-3\gamma}{4\gamma H}\right) p_2\ , \qquad (11)$$

$$F_K = -\frac{B_0}{4\pi}\ < b_x\ v_x >= -\frac{B_0}{4\pi\rho_0^{1/4}} < b_x\ v_1 > \qquad (12)$$

with the transverse (horizontal) magnetic field perturbation, b_x, given by

$$b_x = B_0 \left(\frac{\partial}{\partial t}\right)^{-1} \frac{\partial v_x}{\partial z} = \frac{B_0}{\rho_0^{1/4}} \left(\frac{\partial}{\partial t}\right)^{-1} \left(\frac{\partial}{\partial z} + \frac{1}{4H}\right) v_1 \tag{13}$$

These wave equations can be solved by Fourier transform methods and for example the solution of the transverse wave Eq. (6) is given by

$$v_x(k,\omega) = \frac{1}{(\omega^2 - \omega_K^2) - k^2 c_K^2} \frac{\rho_0^{1/4}}{(2\pi)^2} \frac{\rho_e}{\rho_e + \rho_0} \left[k\omega + \frac{gk}{\omega H} - i\left(\frac{\omega}{H} - \frac{gk^2}{\omega}\right)\right] \times \int\int u_x(z,t) u_z(z,t) e^{-i(\omega t - kz)} dz dt \ . \tag{14}$$

Introducing this solution into Eqs. (12), (13) it is seen that one gets fourth-order velocity correlations $u_x u_z u_x' u_z'$ which can be reduced to second order transverse $u_x u_x'$ and longitudinal $u_z u_z'$ correlations using the properties of isotropic and homogenous turbulence. The convolution integrals involving these second order correlations can be written in terms of a turbulent energy spectrum $E(k,\omega)$, which consists of a spatial and a temporal component

$$E(k,\omega) = E(k)\Delta\left(\frac{\omega}{k u_k}\right) \tag{15}$$

For the spatial component, we take an extended Kolmogorov spectrum given in the following form:

$$E(k) = \begin{cases} 0 & 0 < k < 0.2k_t \\ a\frac{u_t^2}{k_t}\left(\frac{k}{k_t}\right) & 0.2k_t \le k < k_t \\ a\frac{u_t^2}{k_t}\left(\frac{k}{k_t}\right)^{-5/3} & k_t \le k \le k_d \end{cases} \tag{16}$$

which is normalized by

$$\int_0^\infty E(k)dk = \frac{3}{2}u_t^2 \tag{17}$$

Here u_t is the root mean square turbulent velocity $u_t = \sqrt{\overline{u_x(r,t)^2}} = \sqrt{\overline{u_z(r,t)^2}}$ which is identified with the above mentioned convective velocity u from the convection zone model and where one has the spatial frequencies $k_t = 2\pi/H$ and $k_d = 100k_t$ with $a = 0.758$ (Musielak et al. 1994, Theurer, Ulmschneider & Kalkofen 1997). For the temporal component a modified Gaussian frequency factor (Musielak et al. 1994) is taken

$$\Delta\left(\frac{\omega}{k u_k}\right) = \frac{4}{\sqrt{\pi}} \frac{\omega^2}{|k u_k|^3} e^{-(\frac{\omega}{k u_k})^2} \tag{18}$$

where the typical velocity of bubbles of spatial frequency k is given by

$$u_k = \left[\int_k^{2k} E(k')dk'\right]^{1/2} \tag{19}$$

In the numerical approach, which has been employed for the generation of longitudinal and transverse magnetic waves, one first constructs a magnetic flux tube model embedded in a non-magnetic stellar atmosphere and uses a time-dependent wave code (Herbold et al. 1985, Ulmschneider, Zähringer & Musielak 1991) to excite the tube at the bottom with a pressure perturbation p (which translates into a longitudinal velocity perturbation v_z) or a transverse velocity perturbation v_x, all derived from the turbulent velocity fluctuations at that height. These velocity perturbations consist of a superposition of a large number (ca. N=100-500) normal modes of different frequencies ω_n, amplitudes u_n and random phases φ_n

$$v_x(t) = \sum_{n=1}^{N} u_n \sin(\omega_n t + \varphi_n) \quad \text{where} \quad \overline{v_x^2} = u_t^2 = \frac{1}{2}\sum_{n=1}^{N} u_n^2 \tag{20}$$

$$v_z(t) = \frac{c_S^2}{c_T}\frac{p}{\gamma p_0} \quad \text{where} \quad p = \frac{\beta}{2/\gamma+\beta} 3\rho_e(v_x^2 - u_t^2) \tag{21}$$

where $\beta = 8\pi p_0/B_0^2$ (Huang, Musielak & Ulmschneider 1995, Ulmschneider & Musielak 1998, Ulmschneider, Musielak & Fawzy 2001). The velocity amplitudes u_n are evaluated using the extended Kolmogorov energy spectrum (see Eq. 16) and the Gaussian frequency factor (see Eq. 18) of the turbulent flow field. For a given equidistant frequency grid ω_n and the frequency interval $\Delta\omega$, one obtains

$$u_n = \sqrt{\frac{4}{3}\Delta\omega \int_0^\infty E(k)\Delta\left(\frac{\omega_n}{k u_k}\right) dk} \quad . \tag{22}$$

For the root mean square turbulent velocity u_t in this spectrum we take $u_t = u_{max}/2$, where u_{max} is the maximum convective flow speed obtained from the convection zone model. This choice is made because the maximum occurs more than a scale height below the stellar surface where the most efficient excitation of the flux tube waves occurs (Ulmschneider, Musielak & Fawzy 2001).

4. Identification of the heating mechanisms

Having identified various heating processes and the way the mechanical energy is generated, the important question now is which of these mechanisms are the important ones in a stellar and particularly the solar chromosphere and corona. This question to identifying the heating mechanisms has been much debated ever since the discovery of the high coronal temperatures by Grotrian and Edlén around 1941. The persistence of the debate over the many years is due to the fact that despite of the great proximity of the Sun compared to other stars the observation cannot resolve the scales in the meter range where shock dissipation and current sheets operate during the heating process. Thus, for example, a small scale acoustic heating event can always be attributed to unresolved magnetic heating. Surprisingly it is possible to make powerful arguments for the identification of the heating mechanism by employing stellar observations. This is because the stars (main sequence and giant stars) differ only by 4 basic parameters for which one can take g, T_{eff}, Z_m and P_{rot}. The first three were already

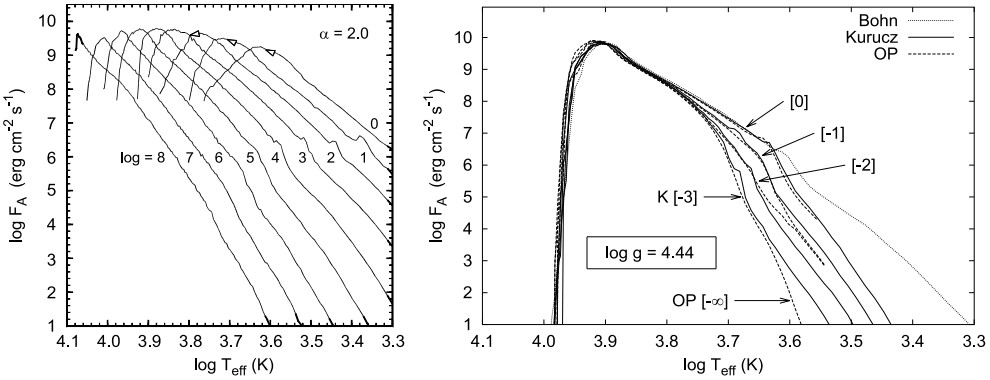

Figure 3. Acoustic flux in stars as function of T_{eff} and g for solar abundances, after Ulmschneider, Theurer & Musielak (1996) (left panel), and for nonsolar abundances Z_m, after Ulmschneider et al. (1999) (right panel).

mentioned above, the fourth is the rotation period. To use stellar observations to identify the heating mechanisms one exploits the strong dependence of the mechanical energy generation on these four basic parameters.

For the acoustic fluxes, P_{rot} does not matter as the convection zones do essentially not depend on rotation. Figure 3 shows the generated acoustic fluxes of stars when the remaining three basic parameters are varied. The left panel of the figure shows that there is a very strong T_{eff} dependence because the acoustic waves in stars are produced by quadrupole sound generation which follows Lighthill's u^8 power law (Lighthill 1952). The strong dependence results from the rapid increase of u with T_{eff}. Giant stars with low gravity g have smaller densities at a given optical depth, such that u must become larger fora given T_{eff} and radiation flux σT_{eff}^4. The right panel at the cool side of the diagram, where the opacity is dominated by metals, shows that the lowering of the metal abundance lowers the opacity which allows the stellar surface to recede to deeper layers, where the density is higher and where the convective velocity u is smaller. However, this effect does not occur on the hot side, where the opacity is dominated by hydrogen.

The acoustic wave energy fluxes and the computed acoustic wave energy spectra (which derive from the turbulent energy spectra) allow to calculate the propagation of acoustic waves into the outer stellar atmospheres where they form shocks (Buchholz & Ulmschneider 1994). This shock formation is a consequence of the strong density decrease in the outer stellar regions which leads to a rapid growth of the wave amplitude. Employing a radiative transfer code to simulate the emergent chromospheric lines from such a shocked heated atmosphere, it is possible to obtain theoretical emerging radiative fluxes for the chromospheric lines of Ca II and Mg II, and then compared these theoretical predictions to observed fluxes measured in the emission cores of these lines (see Cuntz et al. 1999). Such a comparison is shown in Fig. 4.

In Figure 4 the observed emission core fluxes in the Ca II and Mg II lines for main sequence stars (small dots) and giants (triangles) after Rutten et al. (1991)

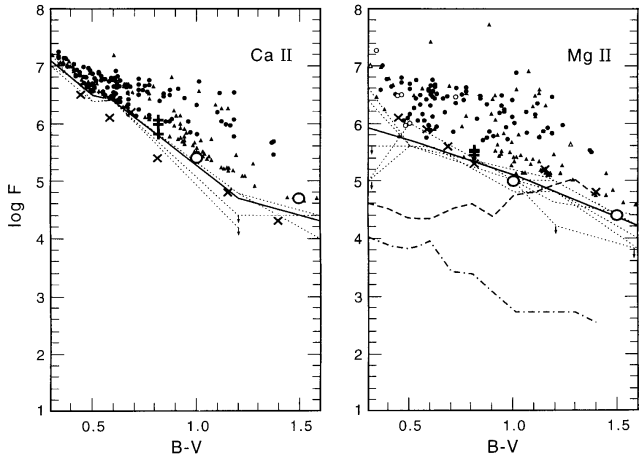

Figure 4. Observed and theoretical core emission fluxes of late type stars together with the empirical basal flux line, modified after Rutten et al. (1991) Buchholz, Ulmschneider & Cuntz (1998), Cuntz & Ulmschneider (1994).

are compared with theoretical simulations of main sequence stars (crosses) and giants (rings) (Buchholz, Ulmschneider & Cuntz 1998) as well as low metallicity stars (plus signs) (Cuntz & Ulmschneider 1994). It is seen that the observations define a lower boundary, the so-called basal flux line, which is independent whether the star is a main sequence star or a giant or whether it has low or high metallicity. These observational facts are reproduced by the theoretical simulations both in terms of the absolute position in the diagram and in terms of the $B-V$ dependence. It must be noted that agreement would not be expected if acoustic waves had nothing to do with the chromospheric heating or if they were only an insignificant fraction of a different (e.g., magnetic) heating mechanism. Figure 4 shows also that there are stars which have much greater emission than the basal flux line. These are stars which rotate more rapidly and are covered with more magnetic regions (Rutten 1986). One thus must conclude that acoustic heating is the basic heating mechanism for the nonmagnetic chromospheres of slowly rotating stars.

Let us now turn to the magnetic heating mechanisms. As discussed above wave energy fluxes and wave energy spectra can be computed for both longitudinal and transverse tube waves. The analytical approach for the generation of longitudinal wave energy fluxes is described by Musielak, Rosner & Ulmschneider (1989, 2000, 2002), Musielak et al. (1995); however, for the numerical approach see Ulmschneider & Musielak (1998), Ulmschneider, Musielak & Fawzy (2001). For transverse wave fluxes using the analytical approach see Musielak & Ulmschneider (2001, 2002a, 2002b), and for the numerical approach see Huang, Musielak & Ulmschneider (1995) with a correction discussed in Ulmschneider & Musielak (1998). Figure 5 displays and compares some of these fluxes.

It is seen that the wave energy fluxes have a much reduced T_{eff} and g dependence and that they depend on the field strength B. In our calcula-

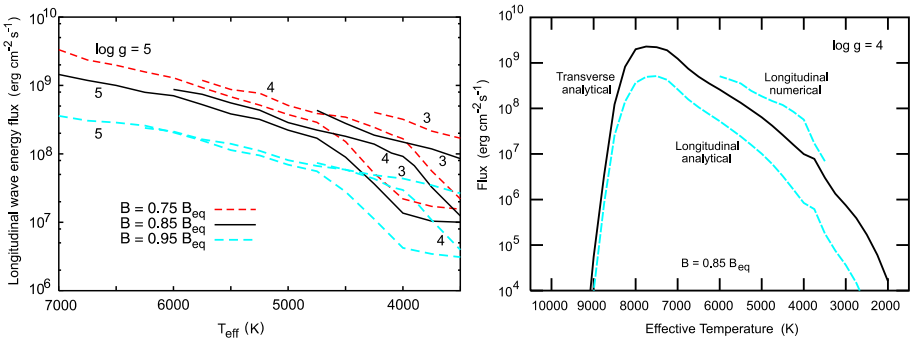

Figure 5. Longitudinal tube wave fluxes (numerical), after Ulmschneider, Musielak & Fawzy (2001) (left), longitudinal and transverse tube wave fluxes, after Musielak & Ulmschneider (2002a)(right).

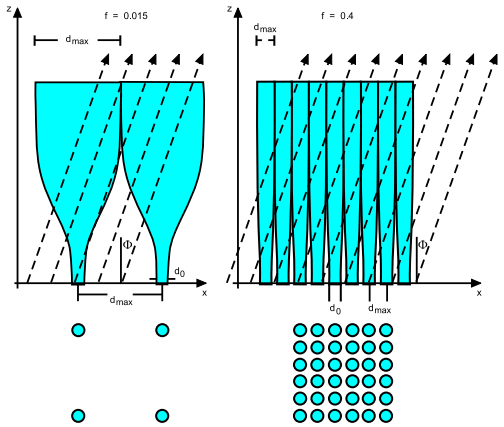

Figure 6. Flux tube models of different filling factors f, for the solar case (left panels) and the case $f = 0.4$ (right panels). The lower panels show the cross-sections at the stellar surface.

tions we specify the field strength in terms of the equipartition field strength $B_{eq} = \sqrt{8\pi p}$, where p is the external gas pressure at the stellar surface. From solar observations, we assume typically field strengths of $B = 0.85 B_{eq}$ for other stars. Increasing the field strength decreases the generated wave flux because it increases the rigidity of the flux tube against external perturbations. One also finds both analytically and numerically that transverse waves are more efficiently generated and that for the Sun this amounts to a factor of about 30. The numerical approach leads to an order of magnitude higher wave energy fluxes (see Fig. 5). This is due to the fact that in the numerical approach frequently large amplitude perturbations arise which produce very spikey waves. This has also been noted elsewhere (Choudhuri, Auffret & Priest 1993a, Choudhuri, Dikpati & Banerjee 1993b).

To understand the magnetic heating mechanisms in stars it is necessary to obtain a model of the field coverage of the star as function of its rotation period P_{rot}. Theoretically this field coverage must depend on only the 4 basic stellar

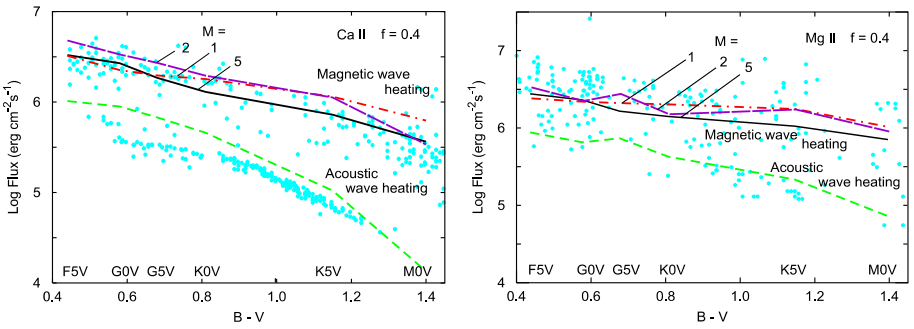

Figure 7. Empirical core emission fluxes of Ca II (dots, left) and Mg II lines (dots, right), compared with theoretical fluxes for pure acoustic wave heating and for magnetic wave heating in flux tubes with an area filling factor of $f = 0.4$.

parameters. Here we sadly miss a first-principle dynamo theory which would give us the required P_{rot} dependence. We get around this problem by assuming that the stars are covered by thin flux tubes of a specified magnetic filling factor f, the fractional area of stellar surface covered by magnetic fields. From the non-rotating stars to the most rapidly rotating ones, we assume that f varies from $f = 0$ to 0.4. Figure 6 shows such idealistic models where the left panels show the solar case and the right panels a star with maximum rotation. The lower panels show the cross-section of the flux tubes (the diameters are equal to a scale height H) at the stellar surface. For $f = 0.4$ the external non-magnetic space with diameter H is barely able to still permit convection to operate and by working on the flux tubes generate tube waves.

Using the longitudinal wave energy fluxes and spectra, wave calculations were performed along the flux tubes as well as the outside medium. The waves form shocks and shock dissipation heats the tubes and the external medium. With a ray tracing multi-dimensional radiative transfer code (Fig. 6), the emergent radiative fluxes in the Ca II and Mg II lines were computed and the core emission fluxes evaluated. Figure 7, taken from Fawzy et al. (2002a, b), shows a comparison for the cases $f = 0$ (labeled acoustic wave heating) and $f = 0.4$ (labeled magnetic wave heating) with observations. The magnetic case shows results from wave computations with different amounts of wave energy added from transverse wave fluxes to the longitudinal fluxes via nonlinear mode-coupling. It is seen that in the case of $f = 0.4$ the theoretical simulations agree with the maximum of the observed emission fluxes for Ca II and to a large degree also for Mg II. This maximum is called saturation limit. The fact that the saturation limit can be reproduced by magnetic wave heating indicates that this mechanism appears to be the additional heating mechanism for magnetic chromospheres. The slight discrepancy between the simulations and the saturation limit for Mg II can be attributed to the fact that the Mg II lines are formed at much greater heights than the Ca II lines. This may simply imply that additional heating is necessary to heat the highest layers of stellar chromospheres and transition regions. It is very likely that either local strong mode coupling

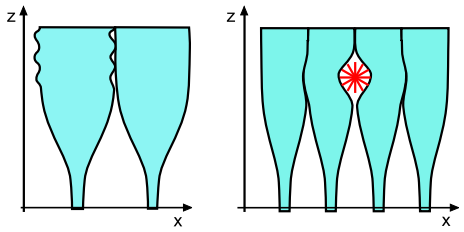

Figure 8. Local intense mode-coupling between tranverse and longitudinal waves (left) and wave heating generated by microflare events (right).

or microflare heating or both (see Fig. 7) operate in these most upper layers of stellar chromospheres.

5. Conclusions

1. Acoustic waves are the main heating mechanism for slowly rotating stars and nonmagnetic regions of stellar chromospheres.
2. Longitudinal tube waves are the main heating mechanism for magnetic flux tubes.
3. Transverse tube waves provide energy for longitudinal waves, the same may be true for torsional waves although the generation rate for the latter has not yet been computed.
4. The solar and stellar chromospheres are heated by waves. The most upper layers of these chromospheres require additional non-wave heating mechanism, possibly by reconnection (microflares).

Acknowledgements This work was supported by NSF under grant ATM-0087184, by NATO under grant CRG-910058, by DFG grant Ul57/34-1 and by the Alexander von Humboldt Foundation.

References

Anderson, L.S. & Athay, R.G. 1989, ApJ, 346, 1010

Buchholz, B. & Ulmschneider, P. 1994, in Cool Stars, Stellar Systems and the Sun, ed. Caillault J.P., (Astr. Soc. Pacific Conf. Ser. 64), 363

Buchholz, B., Ulmschneider, P. & Cuntz, M. 1998, ApJ, 494, 700

Carlsson, M. & Stein, R.F. 1995, ApJ, 440, L29

Choudhuri, A.R., Auffret, H. & Priest, E.R. 1993a, Sol. Phys., 143, 49

Choudhuri, A.R., Dikpati, M. & Banerjee, D. 1993b, ApJ, 413, 811

Cuntz, M., Rammacher, W., Ulmschneider, P., Musielak, Z.E. & Saar, S.H. 1999, ApJ, 522, 1053

Cuntz, M. & Ulmschneider, P. 1994, in Cool Stars, Stellar Systems and the Sun, ed. Caillault J.P., (Astr. Soc. Pacific Conf. Ser. 64), 368

Defouw, R.J. 1976, ApJ, 209, 266

Fawzy, D., Rammacher, W., Ulmschneider, P., Musielak, Z.E. & Stępień, K. 2002, A&A, 386, 971

Fawzy, D., Ulmschneider, P., Stępień, K., Musielak, Z.E. & Rammacher, W. 2002, A&A, 386, 983

Herbold, G., Ulmschneider, P., Spruit, H.C. & Rosner, R. 1995, A&A, 145, 157

Huang, P., Musielak, Z.E. & Ulmschneider, P. 1995, A&A, 297, 579

Lighthill, M.J. 1952, Proc. R. Soc. Lond. A, 211, 564

Musielak, Z.E., Rosner, R., Gail, H.P. & Ulmschneider, P. 1995, ApJ, 448, 865

Musielak, Z.E., Rosner, R., Stein, R.F. & Ulmschneider, P. 1994, ApJ, 423, 474

Musielak, Z.E., Rosner, R. & Ulmschneider, P. 1989, ApJ, 337, 470

Musielak, Z.E., Rosner, R. & Ulmschneider, P. 2000, ApJ, 541, 410

Musielak, Z.E., Rosner, R. & Ulmschneider, P. 2002, ApJ, 573, in press

Musielak, Z.E. & Ulmschneider, P. 2001, A&A, 370, 541

Musielak, Z.E. & Ulmschneider, P. 2002a, A&A, 386, 606

Musielak, Z.E. & Ulmschneider, P. 2002b, A&A, 386, 615

Narain, U. & Ulmschneider, P. 1990, Space Science Reviews, 54, 377

Narain, U. & Ulmschneider, P. 1996, Space Science Reviews, 75, 453

Parker, E.N. 1981, in Solar phenomena in stars and stellar systems, Proc. Adv. Study Inst. Bonas, Bonnet, R.M., Dupree, A.K. Eds., D. Reidel Publ., 33

Parker, E.N. 1991, in Mechanisms of Chromospheric and Coronal Heating, eds. Ulmschneider, P., Priest, E.R. & Rosner, R., Springer Verlag, Heidelberg, 615

Priest, E.R. 1982, Solar magneto-hydrodynamics, D. Reidel, Dordrecht

Rempel, M. 2002, private communication

Rutten, R.G.M. 1986, A&A, 159, 291

Rutten, R.G.M., Schrijver, C.J., Lemmens, A.F.P. & Zwaan, C. 1991, A&A, 252, 203

Stein, R.F. & Nordlund, A. 1991, in Mechanisms of Chromospheric and Coronal Heating, eds. Ulmschneider, P., Priest, E.R. & Rosner, R., Springer Verlag, Heidelberg, 386

Theurer, J., Ulmschneider, P. & Kalkofen, W. 1997, A&A, 324, 717

Ulmschneider, P. 1996, in Cool Stars, Stellar Systems and the Sun, eds. Pallavicini, R. and Dupree, A.K. (Astr. Soc. Pacific Conf. Ser. 109), 71

Ulmschneider, P., Fawzy D., Musielak Z.E. & Stępień K. 2001, ApJ, 559, L167

Ulmschneider, P. & Musielak, Z.E. 1998, A&A, 338, 311

Ulmschneider, P., Musielak, Z.E. & Fawzy, D.E. 2001, A&A, 374, 662

Ulmschneider, P., Theurer, J. & Musielak, Z.E. 1996, A&A 315, 212

Ulmschneider, P., Theurer, J., Musielak, Z.E. & Kurucz, R. 1999, A&A, 347, 243

Ulmschneider, P., Zähringer, K. & Musielak, Z.E. 1991, A&A, 241, 625

Withbroe, G., & Noyes, R.W. 1977, Ann. Rev. Astr. Ap., 15, 363